Downloaded from jnm.snmjournals.org by on March 14, 2017. For personal use only.

Correlation Between PET and SISCOM in Temporal Lobe Epilepsy

Viviane Bouilleret, MD, PhD[1,2]; M. Paola Valenti, MD[3]; Edouard Hirsch, MD[3]; Franck Semah, MD[1]; and Izzie J. Namer, MD, PhD[4]

[1]Service Hospitalier Frédéric Joliot, Commissariat à l'Energie Atomique, Orsay, France; [2]Service d'Explorations du Système Nerveux Central, Centre Hospitalier Universitaire du Kremlin Bicètre, Paris, France; [3]Unité d'Explorations Fonctionnelles des Epilepsies, Clinique Neurologique, Centre Hospitalier Universitaire de Strasbourg, France; and [4]Faculté de Médecine, Institut de Physique Biologique, Strasbourg, France

The subtraction of interictal from ictal SPECT coregistered to 3-dimensional (3D) MRI (SISCOM) and ^{18}F-FDG PET are 2 techniques that are involved in the definition of the epileptogenic zone in refractory partial temporal lobe epilepsy (TLE). The aim of this study was compare, region by region, the functional patterns obtained by both strategies, SISCOM and PET, in patients with unilateral TLE. **Methods:** Perfusion data using SISCOM and metabolic data using ^{18}F-FDG PET scans were acquired from 17 patients with unilateral TLE. The functional metabolism and perfusion maps were overlaid onto a 3D rendering of the patient's anatomic MRI scans. **Results:** The functional patterns that were observed with PET and SISCOM were found mainly in the ipsilateral and contralateral temporal lobes, in the orbitofrontal and insular cortices. Despite the high rate of concordance, in some cases discrepancies could be observed between PET and SISCOM abnormalities: In the mesial regions, as in the anterior neocortex, PET abnormalities were found more frequently than SISCOM changes. SISCOM abnormalities were found more frequently in the posterior temporal neocortex. In the extratemporal cortex, SISCOM abnormalities were more widespread. **Conclusion:** The marked rate of concordance between PET and SISCOM abnormalities observed in relatively extensive regions shows that, in TLE, seizures were generated and spread in metabolically abnormal regions.

Key Words: temporal lobe epilepsy; PET; SPECT

J Nucl Med 2002; 43:991–998

The potentials of noninvasive functional strategies to localize the epileptogenic zone in refractory temporal lobe epilepsy (TLE) have become well established in the diagnostic evaluation of TLE patients considered for epilepsy surgery (*1*,*2*). PET studies with ^{18}F-FDG have provided evidence of interictal hypometabolism in the epileptogenic zone, with a sensitivity of 70%–90% (*2*–*6*). Ictal SPECT and, more recently, the subtraction of interictal from ictal SPECT coregistered to 3-dimensional (3D) MRI (SISCOM) have been used to image cerebral perfusion during seizures. SPECT hyperperfusion has been clearly shown (*7*–*11*) to be a highly sensitive technique for the localization of an epileptogenic zone.

Although both functional strategies have been used primarily in the presurgical evaluation of TLE, and their potentials evaluated individually, the correspondence between local interictal hypometabolism and hyperperfusion occurring during a seizure in the same patient has never been clearly evaluated. The few studies (*12*–*15*) broaching this subject were based on a global approach—that is, on laterality or on rough localization concordance (temporal vs. extratemporal injury). The aim of this study was to establish, region by region, the concordance rates of these 2 noninvasive techniques in the evaluation of temporal and extratemporal consequences in unilateral TLE. Recent studies have shown that increased glucose metabolism (*16*) or decreased cerebral blood flow (*17*–*19*) could be noted in the epileptogenic cortical areas. In this study, we have compared only the interictal hypometabolism pattern with the ictal hyperperfusion pattern.

MATERIALS AND METHODS

Patients

The population studied included 17 patients with medically refractory epilepsy of temporal lobe origin who were undergoing presurgical evaluation (Table 1). Each patient underwent ^{18}F-FDG PET and SISCOM in the presurgical evaluation. In addition, all patients underwent identical evaluation including medical, neurologic, and neuropsychologic examinations; video-electroencephalographic (EEG) monitoring; and brain MRI examinations. The patient selection criteria for this analysis included medically intractable unilateral TLE based on seizure semiology and ictal EEG studies and absence of visually detectable contralateral abnormality on high-resolution MRI.

PET Data Acquisition

^{18}F-FDG PET studies were performed using a high-resolution head-dedicated PET camera (ECAT 953/31B; Siemens Medical Systems, Iselin, NJ). This tomograph has a 5.8-mm in-plane and 5-mm axial resolution (*20*). For each patient, 31 transverse sec-

Received Oct. 23, 2001; revision accepted Mar. 26, 2002.

For correspondence or reprints contact: Izzie J. Namer, MD, PhD, Faculté de Médecine, Institut de Physique Biologique, 4, rue Kirschleger, 67085 Strasbourg Cedex, France.

E-mail: namer@ipb.u-strasbg.fr

Downloaded from jnm.snmjournals.org by on March 14, 2017. For personal use only.

TABLE 1
Study Population

Patient no.	Age (y)	Sex	History			Electroclinical data		Surgery	MRI or neuropathologic data	SPECT	
			Febrile convulsion	Age at onset (y)	Seizure frequency (no./mo)	Lateralization	sEEG			Length of seizure in ictal SPECT (s)	Injection delay of ^{99m}Tc-ECD (s)
1	44	M	Yes	5	30	L temporal			L dysplasia (pole) + HS	126	59
2	30	M	Yes	7	2	L temporal	Yes	Yes	L HS	60	16
3	47	F		13	60	L temporal		Yes	L DNT (amygdala)	106	27
4	43	M	Yes	6	30	R temporal		Yes	R HS	87	19
5	29	F	Yes	12	8	R temporal			R HS	70	28
6	35	F		15	2	R temporal		Yes	R cavernoma (T4)	82	7
7	21	M	Yes	2	30	R temporal		Yes	R HS	80	44
8	40	F		6	10	L temporal		Yes	L HS	131	34
9	41	F		11	12	L temporal	Yes		L HS	190	26
10	25	M		7	8	L temporal		Yes	L HS	180	12
11	50	M	Yes	34	15	R temporal		Yes	R HS	110	10
12	34	F		12	3	R temporal		Yes	R HS	88	10
13	26	M	Yes	10	3	R temporal	Yes	Yes	R HS	92	13
14	68	F		25	2	R temporal			R HS	60	7
15	19	M	Yes	3	12	R temporal	Yes	Yes	R cavernoma (cingulum) + HS	120	28
16	24	F	Yes	9	10	R temporal	Yes	Yes	R HS	100	20
17	49	M	Yes	4	3	R temporal		Yes	R HS	80	30

sEEG = stereo-electroencephalography; ECD = ethylcysteinate dimer; HS = hippocampal sclerosis; DNT = dysembryoplastic neuroepithelial tumor.

tions of the brain, 3.4 mm apart, were acquired simultaneously. ^{18}F-FDG was injected intravenously at a mean dose of 207 MBq/70 kg of body weight. Image acquisition was started 30 min after the ^{18}F-FDG injection and ended 20 min later. PET scanning and injection of the tracer were conducted in a quiet, dimly lit environment with minimal background noise. The subjects were studied in an awake resting state, with eyes closed and ears unplugged. During PET scanning the patients were carefully monitored for head movements. Reconstructed images were corrected for attenuation using ^{68}Ga–^{68}Ge transmission scans. These investigations took place during an interictal phase, ascertained by close clinical supervision.

Before each PET study, the plane parallel to the long axis of the hippocampus was determined individually on a T1-weighted 7-mm-thick parasagittal MR image as described (*21*). Briefly, the angle between the MR axial plane and the hippocampal plane was determined and then recorded on the patient's head with skin markers. The head of the subject was then tilted in the MRI head holder. To obtain a set of MRI scans superimposable on the PET images, contiguous axial T1-weighted slices were then performed in the hippocampal plane with a special 3.4-mm-thick slice interval (25-cm field of view, 256^2 data matrix). PET images were then replaced on MR images using an automatic 3D registration method (Fig. 1) (*22*). In all cases, regional metabolic values were normalized to the global cerebral activity.

SISCOM Data Acquisition

SPECT imaging studies were realized with a low-energy, high-resolution, double-head camera (Helix; Elscint, Haifa, Israel) using 740–925 MBq ^{99m}Tc-ethylcysteinate dimer ([ECD] Neurolite; DuPont Pharma, North Billerica, MA). The camera was operated in the stop-and-shoot mode, with acquisitions at 3° intervals and a total acquisition time of 30 min (120 projections, 642 matrix). The total number of counts was 5 million. Slices were reconstructed by filtered backprojection using a Metz filter (full width at half maximum, 8 mm). The interictal studies were performed after a 24-h seizure-free period. Video-EEG recording was used before and during isotope injection. For ictal studies, patients underwent continuous video-EEG monitoring and the isotope was injected immediately after the clinical onset of a seizure. Slices were acquired 30 min after the injection of ECD. The MR studies used for SISCOM were obtained with a 3D inversion-recovery gradient-echo sequence, using a 25.6-cm field of view and a 128^3 matrix. SISCOM images were obtained on a C360 workstation (Hewlett-Packard, Andover, MA) using the 3D medical image analysis software MEDIMAX (http://www-ipb.u-strasbg.fr/ipb/gitim). The procedure consisted of 3 steps:

- SPECT–MRI registration. The ictal and interictal SPECT images were registered successively on the MRI using a fully automated data-driven registration algorithm. This algorithm relies on a robust voxel similarity-based method that enables accurate rigid registration of dissimilar multimodal 3D images (*23*).
- Ictal − interictal difference. To obtain the difference SPECT, interictal SPECT images were first subtracted from ictal SPECT images; each voxel value of this subtracted image was then divided by the mean voxel value of the interictal SPECT. The result was represented as a percentage of cerebral perfusion variation relative to the interictal SPECT.

Downloaded from jnm.snmjournals.org by on March 14, 2017. For personal use only.

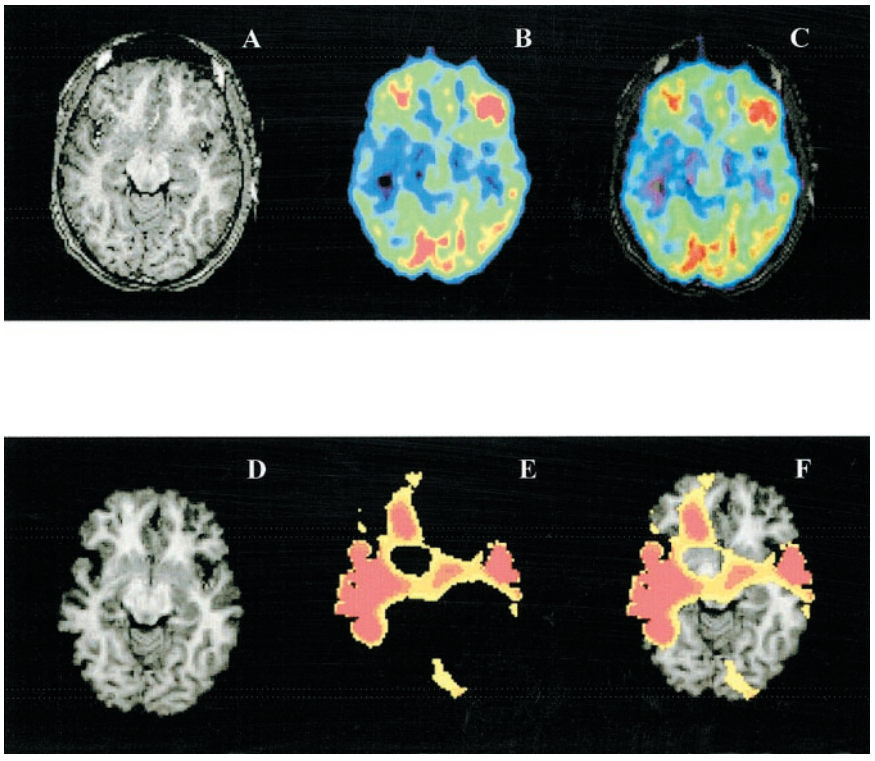

FIGURE 1. Images of representative patient. (A–C) First MRI (A), PET (B), and superimposed MRI–PET (C). (D–F) Second MRI obtained for SISCOM (D), difference SPECT (E), and SISCOM (F).

- Fusion of MRI and difference SPECT images (SISCOM). In this study only positive variations have been retained to create the SISCOM images (Fig. 1).

Data Analysis

All neuroimaging findings were interpreted independently by 2 experienced specialists without prior knowledge about the results of electroclinical data. PET and SISCOM images were interpreted on the basis of qualitative visual analysis, which took into account several regions, including the temporal lobes, perisylvian regions, frontal lobes, posterior regions, and subcortical structures. Regarding the PET studies, the area with the greatest decrease in ^{18}F-FDG uptake relative to the intra- and interhemispheric metabolic patterns was considered as the hypometabolic region. With respect to the SISCOM studies, perfusion variations of ≥10% were regarded as significant. Interobserver reliability was tested with a κ-test, which showed an excellent agreement regarding the localization of abnormalities ($\kappa = 0.96$). The interrater concordance was 98% (1335/1360 regions). In case of disagreement, both specialists reviewed the scans and a consensus was obtained. The final results are expressed as a percentage of the number of patients in whom abnormalities have been found, either with PET and SISCOM, PET alone, or SISCOM alone.

RESULTS

Temporal Abnormalities

In the ipsilateral hemisphere, mesial and polar functional abnormalities were present in all patients, with the higher rate of concordance between PET and SISCOM (82% and 100%, respectively) (Figs. 2A and 2B). In the ipsilateral anterior temporal neocortex (Figs. 2B, 3A, and 3C), functional abnormalities were found in >94% of the patients (superior and middle temporal gyri = 94%; inferior temporal gyrus = 100%). The concordance between PET and SISCOM also remained high in the anterior temporal neocortex (superior and middle temporal gyri = 70.6%; inferior temporal gyrus = 65%). The discrepancy between PET and SISCOM abnormalities was in favor of PET, in the mesial regions as in the anterior neocortex. In the ipsilateral posterior temporal neocortex (Figs. 2D, 3B, and 3D), the rate of abnormalities rose to >80%, with a concordance rate of 39% between PET and SISCOM. In case of discrepancy between PET and SISCOM, SISCOM abnormalities were more frequent. In the temporal contralateral side, functional abnormalities occurred mainly in the mesial regions (85%) and in the polar region (76%) but also in the anterior temporal neocortex (57%) and in the posterior neocortex (29%). The rate of correlation between PET and SISCOM in the anterior mesial region reached 65%. In case of discrepancy between PET and SISCOM, PET abnormalities alone were more frequent in the anterior temporal regions. Conversely, in the posterior temporal neocortex, SISCOM abnormalities were the most frequent.

Frontal Abnormalities

Frontal functional abnormalities occurred mainly in the ipsilateral and contralateral orbitofrontal gyrus, with a high rate of concordance between PET and SISCOM (Fig. 4A). Abnormalities could also extend to the cingulate gyrus and, to a lesser extent, to the prefrontal cortex and the polar region. Most of these functional changes were evident

Downloaded from jnm.snmjournals.org by on March 14, 2017. For personal use only.

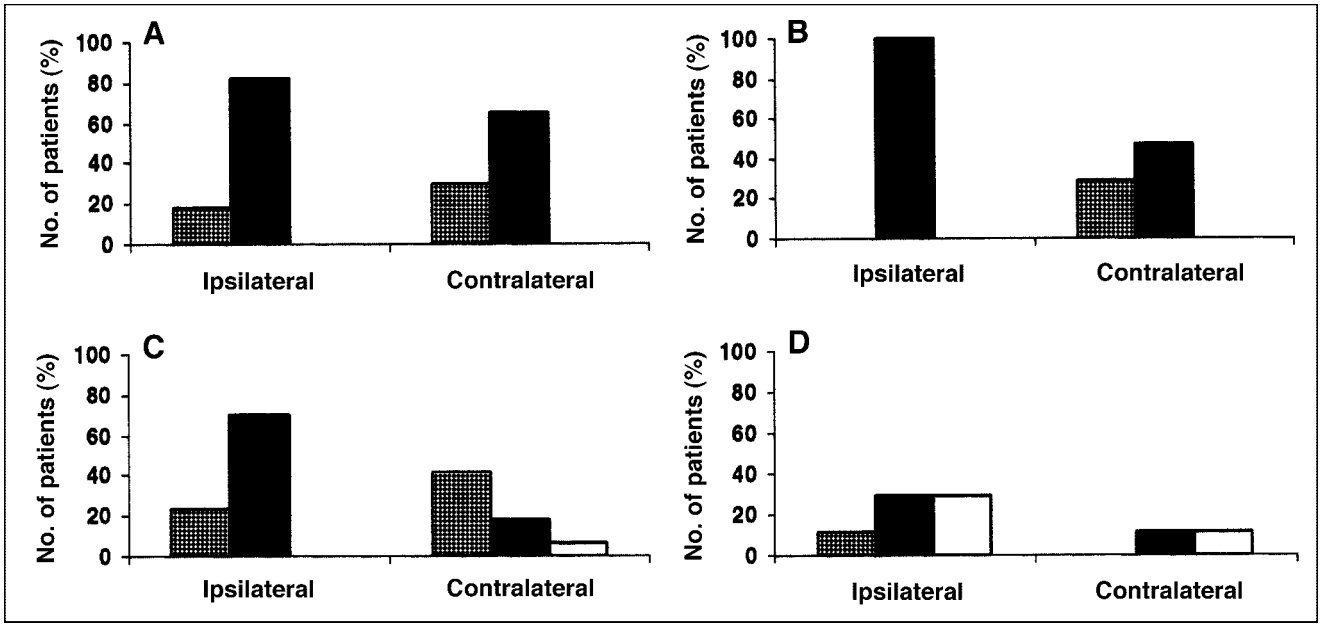

FIGURE 2. PET and SISCOM abnormalities in ipsilateral and contralateral temporal lobe (■, PET and SISCOM abnormalities; ▨, PET abnormalities alone; □, SISCOM abnormalities alone). (A) Mesial temporal structures. (B) Temporal pole. (C) Anterior part of superior temporal gyrus. (D) Posterior part of superior temporal gyrus.

mainly with SISCOM in the ipsilateral and contralateral lobe (Figs. 4B and 4D).

Perisylvian Abnormalities

Functional changes in the insular gyri occurred on the ipsilateral and contralateral sides (Fig. 4C), with a high rate of concordance between PET and SISCOM. Functional changes were also found in the pre- and postcentral gyri on both sides. In these regions, the rate of abnormalities revealed on PET and SISCOM or SISCOM alone was similar (Figs. 5A and 5B).

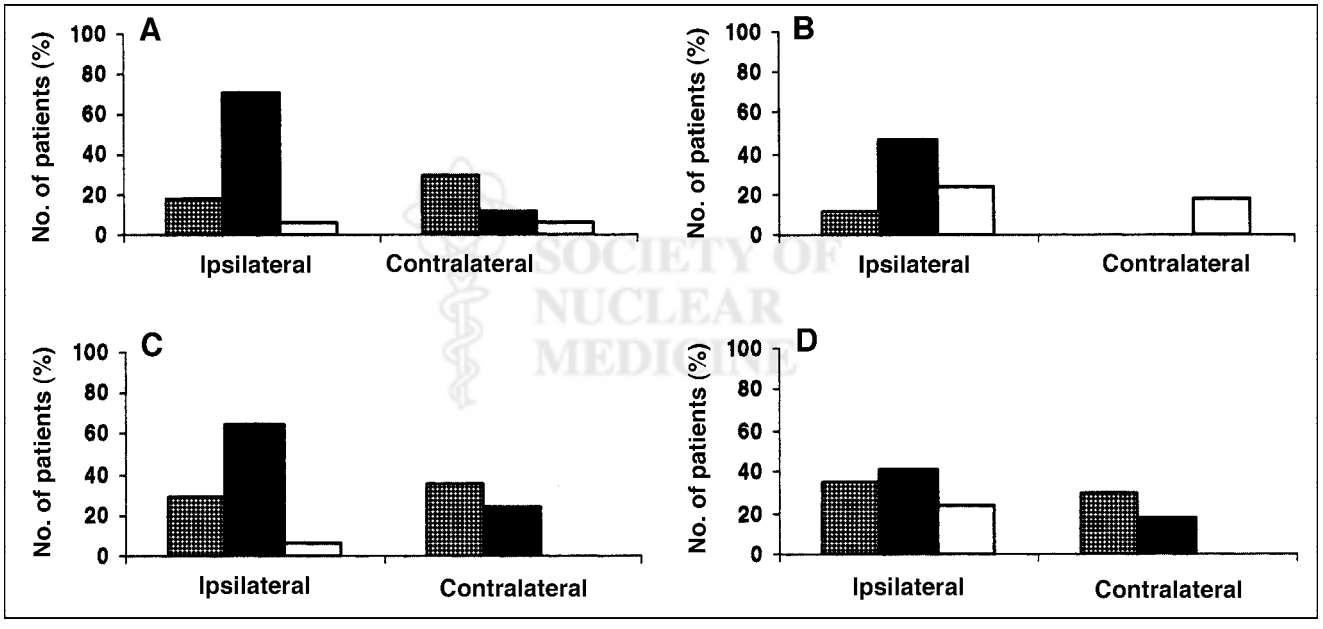

FIGURE 3. PET and SISCOM abnormalities in ipsilateral and contralateral temporal lobe (■, PET and SISCOM abnormalities; ▨, PET abnormalities alone; □, SISCOM abnormalities alone). (A) Anterior part of middle temporal gyrus. (B) Posterior part of middle temporal gyrus. (C) Anterior part of inferior temporal gyrus. (D) Posterior part of inferior temporal gyrus. Functional changes occurred mainly in polar, mesial, and anterior ipsilateral regions. Polar region displayed higher rate of concordance between PET and SISCOM. In cases of discrepancy between PET and SISCOM, functional changes were in favor of PET in mesial and anterior temporal neocortex. Conversely, in posterior part of temporal gyrus, SISCOM abnormalities alone were more frequent. Note involvement of contralateral side in same way but to lesser extent.

Downloaded from jnm.snmjournals.org by on March 14, 2017. For personal use only.

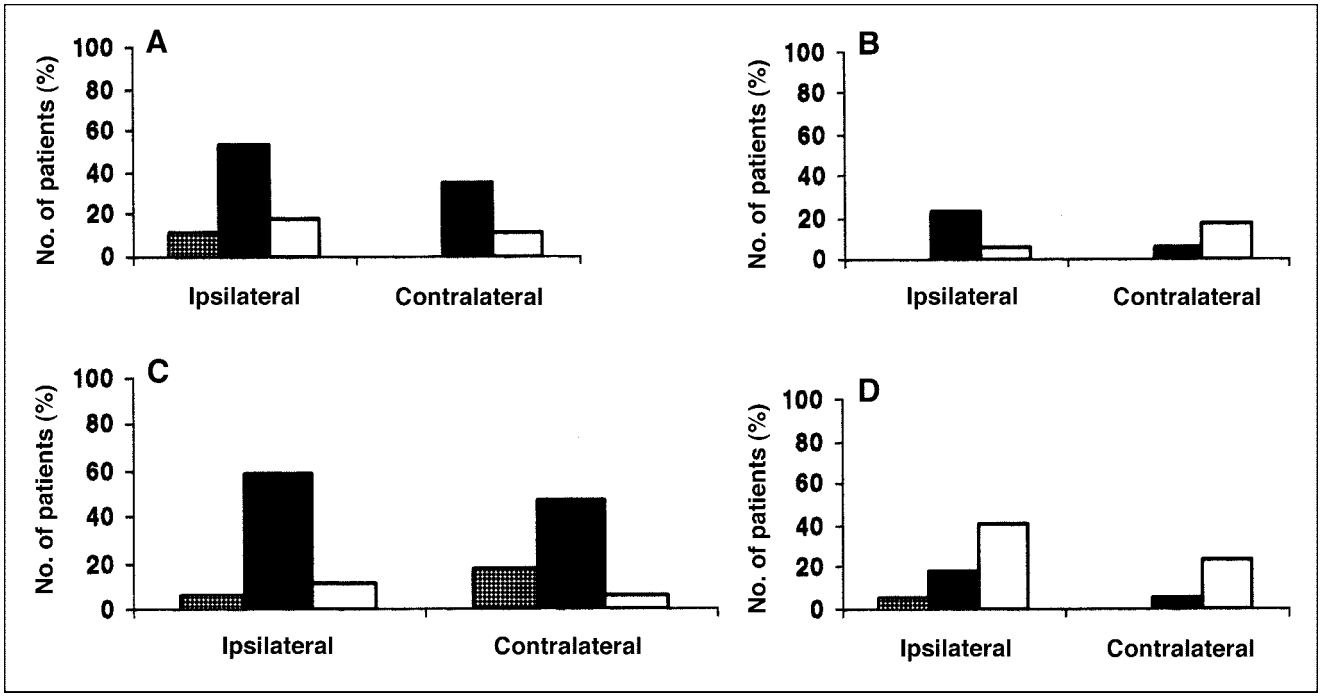

FIGURE 4. PET and SISCOM abnormalities in ipsilateral and contralateral frontal and perisylvian regions (■, PET and SISCOM abnormalities; ▨, PET abnormalities alone; □, SISCOM abnormalities alone). (A) Orbitofrontal gyri and gyrus rectus. (B) Frontal pole and prefrontal cortex. (C) Insular gyri. (D) Cingulate gyrus. Note marked involvement of ipsilateral and contralateral orbitofrontal gyrus (A) and insular cortex (C) with high rate of concordance between PET and SISCOM. In cases of spreading functional changes, SISCOM abnormalities were more frequent (B and D).

Posterior Abnormalities

Functional changes occurred also on both sides in the parietal region, the temporo–parieto–occipital junction and the occipital cortex (Figs. 5C, 5D, and 6A). On the ipsilateral side, the rate of concordance between PET and SISCOM was similar in all of these anatomic regions, except in the occipital cortex, where SISCOM changes were higher. On the contralateral side, mainly SISCOM abnormalities were observed, whereas almost no changes were observed with PET alone.

Subcortical Abnormalities

On the ipsilateral side, functional abnormalities involving the basal ganglia were noted in the caudate nucleus and in the lenticular nucleus in 47% and 82.3% of the patients, respectively, which were more frequently detected using SISCOM alone (Figs. 6C and 6D). Thalamic functional changes were found in 76.4% of the patients, and 35.3% of these anomalies were detected with SISCOM and PET, and 29.4% were detected with only SISCOM (Fig. 6B). On the contralateral hemisphere, functional abnormalities in the basal ganglia were noted to a lesser extent than on the ipsilateral side. As in the other hemisphere, these changes were revealed primarily with only SISCOM. Thalamic functional changes were found in 64.7% of the patients, with abnormalities also observed primarily with SISCOM alone.

DISCUSSION

The main result of this study is the marked rate of concordance between PET and SISCOM abnormalities in patients with TLE with a unilateral lesion. The similarity between the results was found despite the numerous factors that can influence SISCOM data, such as heterogeneity of the ictal symptoms or heterogeneity of the imaging timing (pure ictal or early postictal), which depends on the duration of the seizures and on the uptake properties of the tracer (i.e., uptake after the injection delay and the first pass of blood through the brain capillaries, ~15 s). In this study the functional patterns observed with PET and SISCOM occurred mainly in the ipsilateral and contralateral temporal lobes, in the orbitofrontal gyrus, and in the insular cortex.

In agreement with previous studies (*7,24–27*), the functional changes observed in this study involved predominantly the temporal lobe but spread further out, mainly to the orbitofrontal and insular cortices. Moreover, in these regions, there is a marked correspondence between interictal hypometabolism and ictal hyperperfusion. The concordance between PET and SISCOM is 100% in the polar region; 73.6% in the ipsilateral, mesial, and anterior temporal neocortex; and 65% in the contralateral mesial region. The high rate of polar involvement underlines its predominant role in TLE (*28–31*). The polar region has been shown to be involved at the onset of temporal lobe seizures, which could

Downloaded from jnm.snmjournals.org by on March 14, 2017. For personal use only.

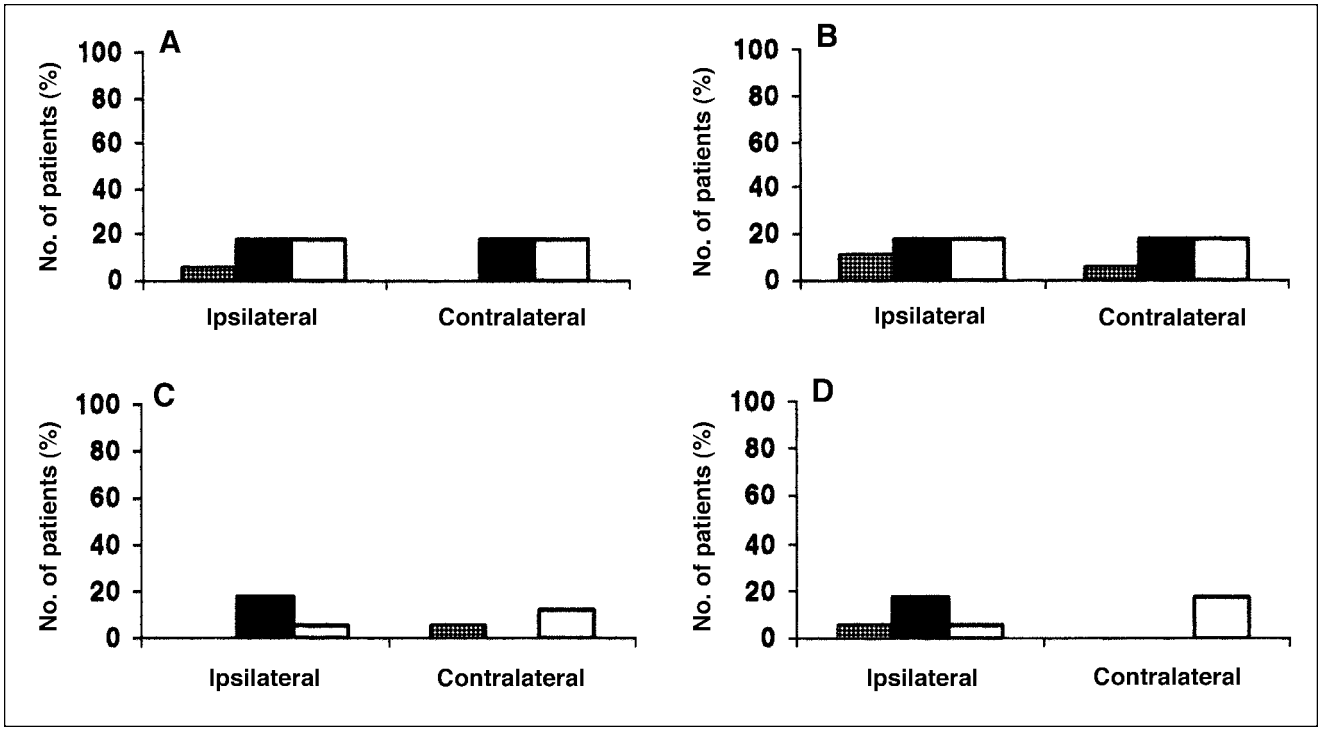

FIGURE 5. PET and SISCOM abnormalities in ipsilateral and contralateral central and posterior regions (■, PET and SISCOM abnormalities; ▨, PET abnormalities alone; □, SISCOM abnormalities alone). (A) Precentral gyrus. (B) Postcentral gyrus. (C) Superior and inferior parietal gyri. (D) Temporo–parieto–occipital junction. Rate of concordance between PET and SISCOM in pre- and postcentral cortex (A and B), parietal region (C), and temporo–parieto–occipital junction (D) is similar. In cases of discrepancy between these examinations, SISCOM abnormalities were found to predominate.

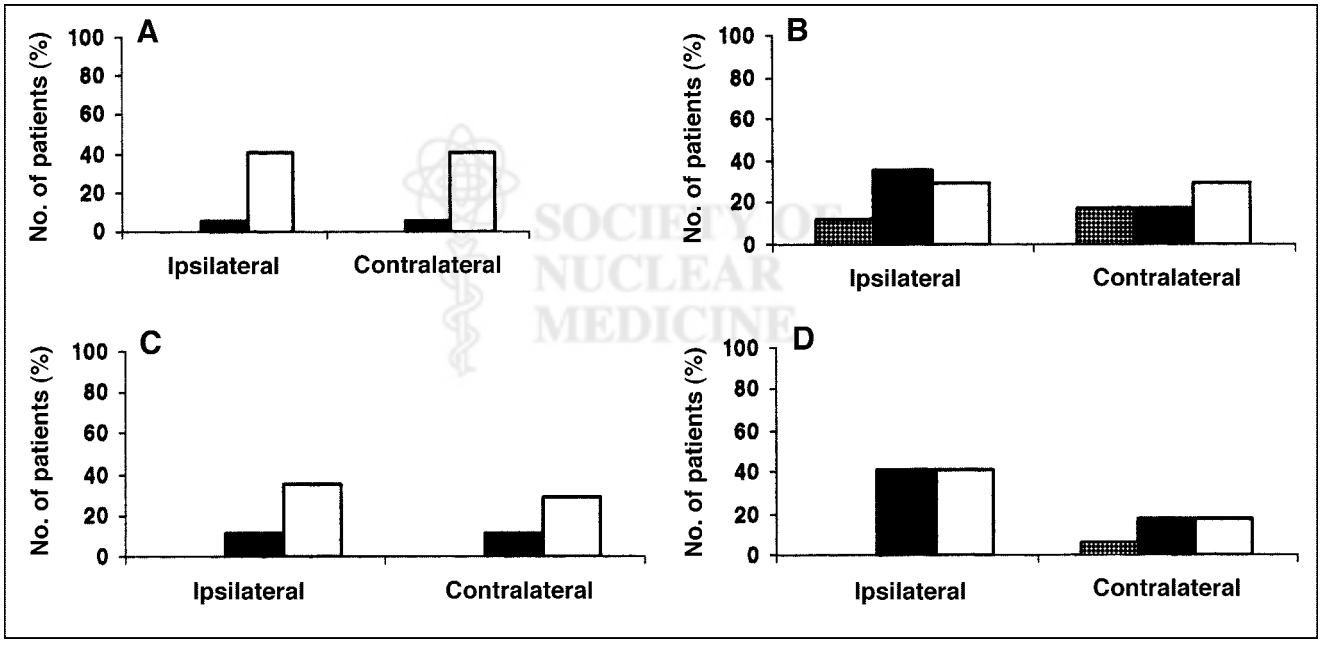

FIGURE 6. PET and SISCOM abnormalities in ipsilateral and contralateral occipital and subcortical regions (■, PET and SISCOM abnormalities; ▨, PET abnormalities alone; □, SISCOM abnormalities alone). (A) Occipital cortex. (B) Thalamus. (C) Caudate nucleus. (D) Lenticular nucleus. SISCOM revealed mainly functional changes in basal ganglia (C and D) and thalamus (B). Such changes occurred in ipsilateral and contralateral hemispheres. SISCOM abnormalities were found to predominate in occipital regions (A).

Downloaded from jnm.snmjournals.org by on March 14, 2017. For personal use only.

explain failure of selective amygdalohippocampectomy. The correlation rate between PET and SISCOM remains high outside the temporal lobe, with 53% in the orbitofrontal cortex and the insula. Such a similar pattern between interictal hypometabolism and ictal hyperperfusion suggests a persistent dysfunction in these highly connected anatomic regions (*32*,*33*). Thus, interictal dysfunction, observed in the anterior part of the temporal lobe, the orbitofrontal region, and the insula cortex, exists in most patients with TLE and shares a predominant part in the epileptogenic network.

In the mesial and the anterior temporal neocortex, PET hypometabolism is more frequent than SISCOM hyperperfusion. Because only SISCOM hyperperfusion has been considered in our study, hypoperfusion has been neglected. This relative discrepancy between PET and SISCOM changes in the epileptic focus can be in relation to seizure propagation (*19*). In fact, ictal SPECT represents the perfusion status when the radiotracer is being injected. During the ictal period, the regional cerebral flow continues to change because ictal discharge propagates. Thus, the initial ictal zone could show hypoperfusion due to intraictal early exhaustion or a steal phenomenon from neighboring brain regions where ictal discharges are propagated, whereas hyperperfusion would appear in the subsequently active zone where ictal discharges build up. This explains the higher rate of SISCOM abnormalities in the posterior temporal region compared with PET data in our study. In the ipsilateral posterior temporal neocortex and outside the temporal lobe, SISCOM hyperperfusion was more widespread than PET changes in most patients. This finding probably reflects the dynamic aspect of the seizure diffusion (recorded with SISCOM) influenced by the duration of the seizure, the propagation speed, and the pathway of ictal EEG discharges. The variable moment of injection during the ictal SPECT could also play a role (*10*,*12*,*34*). Contralateral SISCOM abnormalities probably reflect seizure propagation from the ipsilateral hemisphere through the commissural fibers.

Seizure propagation is also underlined by subcortical involvement (*35*–*38*). Previous studies have suggested the involvement of the basal ganglia and thalamus in the initiation or the propagation of temporal lobe seizures. Simultaneous intracranial thalamic or basal ganglia and temporal EEG recordings during seizure activity have shown electrographic abnormalities involving the subcortical structures (*39*). It remains possible that thalamic activity could regulate epileptic activity in TLE. Such a hypothesis is supported by increased thalamic synaptic activity during vagus nerve stimulation, producing antiseizure effects (*40*). Subcortical involvement during the ictal phase could provide preferential pathways for the propagation of ictal activity from mesial sites and could regulate the excitability of the side to which seizures spread (*39*).

CONCLUSION

Interictal hypometabolic areas correlate very well with ictal hyperperfused regions in TLE (such as ipsilateral and contralateral temporal, orbitofrontal, and insular regions). Do all of these regions correspond to the epileptogenic zone? Further studies with stereo-EEG correlation are necessary to answer this question, which is important from a surgical point of view.

ACKNOWLEDGMENTS

The assistance of the Epilepsy Unit (Strasbourg), PET (Commissariat à l'Energie Atomique, Orsay), and Nuclear Medicine (Strasbourg) staff in acquiring data are gratefully acknowledged. The authors also thank Nathalie Heider for correcting the English. This work was supported by a grant from the Commissariat à l'Energie Atomique, the Hôpitaux Universitaires de Strasbourg, and the Université Louis Pasteur.

REFERENCES

1. Duncan JS. Imaging and epilepsy. *Brain.* 1997;120:339–377.
2. Spencer SS. The relative contributions of MRI, SPECT and PET imaging in epilepsy. *Epilepsia.* 1994;35(suppl 6):S72–S89.
3. Henry TR, Chugani HT, Abou-Khalil BW, Theodore WH, Swartz BE. Positron emission tomography. In: Engel J Jr, ed. *Surgical Treatment of the Epilepsies.* New York, NY: Raven Press; 1993:211–232.
4. Engel J Jr. Update on surgical treatment of the epilepsies: summary of the Second International Palm Desert Conference on the Surgical Treatment of the Epilepsies (1992). *Neurology.* 1993;43:1612–1617.
5. Drzezga A, Arnold S, Minoshima S, et al. ^{18}F-FDG PET studies in patients with extratemporal and temporal epilepsy: evaluation of an observer-independent analysis. *J Nucl Med.* 1999;40:737–746.
6. Juhasz C, Chugani DC, Muzik O, et al. Is epileptogenic cortex truly hypometabolic on interictal positron emission tomography? *Ann Neurol.* 2000;48:88–96.
7. Brinkmann BH, O'Brien TJ, Aharon S, et al. Quantitative and clinical analysis of SPECT image registration for epilepsy studies. *J Nucl Med.* 1999;40:1098–1105.
8. Spanaki MV, Spencer SS, Corsi M, Macmullan J, Seibyl J, Zubal IG. Sensitivity and specificity of quantitative difference SPECT analysis in seizure localization. *J Nucl Med.* 1999;40:730–736.
9. Vera P, Kaminska A, Cieuta C, et al. Use of subtraction ictal SPECT co-registered to MRI for optimizing the localization of seizure foci in children. *J Nucl Med.* 1999;40:786–792.
10. Lee JD, Kim HJ, Lee BI, Kim OK, Jeon TJ, Kim MJ. Evaluation of ictal brain SPECT using statistical parametric mapping in temporal lobe epilepsy. *Eur J Nucl Med.* 2000;27:1658–1665.
11. Shin WC, Hong SB, Tae WS, Seo DW, Kim SE. Ictal hyperperfusion of cerebellum and basal ganglia in temporal lobe epilepsy: SPECT subtraction with MRI coregistration. *J Nucl Med.* 2001;42:853–858.
12. Ho SS, Berkovic SF, Berlangieri SU, et al. Comparison of ictal SPECT and interictal PET in the presurgical evaluation of temporal lobe epilepsy. *Ann Neurol.* 1995;37:738–745.
13. Markand ON, Salanova V, Worth R, Park HM, Wellman HN. Comparative study of interictal PET and ictal SPECT in complex partial seizures. *Acta Neurol Scand.* 1997;95:129–136.
14. Won HJ, Chang KH, Cheon JE, et al. Comparison of MR imaging with PET and ictal SPECT in 118 patients with intractable epilepsy. *Am J Neuroradiol.* 1999; 20:593–599.
15. Hwang SI, Kim JH, Park SW, et al. Comparative analysis of MR imaging, positron emission tomography, and ictal single-photon emission CT in patients with neocortical epilepsy. *Am J Neuroradiol.* 2001;22:937–946.
16. Bittar RG, Andermann F, Olivier A, et al. Interictal spikes increase cerebral glucose metabolism and blood flow: a PET study. *Epilepsia.* 1999;40:170–178.
17. Avery RA, Zubal IG, Stokking R, et al. Decreased cerebral blood flow during seizures with ictal SPECT injections. *Epilepsy Res.* 2000;40:53–61.
18. Kahane P, Merlet I, Grégoire MC, Munari C, Perret J, Mauguière F. An $H_2{}^{15}O$-PET study of cerebral blood flow changes during focal epileptic discharges induced by intracerebral electrical stimulation. *Brain.* 1999;122:1851–1865.

Downloaded from jnm.snmjournals.org by on March 14, 2017. For personal use only.

19. Lee HW, Hong SB, Tae WS. Opposite ictal perfusion patterns of subtracted SPECT: hyperperfusion and hypoperfusion. *Brain.* 2000;123:2150–2159.
20. Mazoyer B, Trebossen R, Deutch R, Casey M, Blohm K. Physical characteristics of the ECAT 953B/31: a new high resolution brain positron tomograph. *IEEE Trans Med Imaging.* 1991;10:499–504.
21. Semah F, Baulac M, Hasboun D, et al. Is interictal temporal hypometabolism related to mesial temporal sclerosis? A positron emission tomography/magnetic resonance imaging confrontation. *Epilepsia.* 1995;36:447–456.
22. Mangin JF, Frouin V, Bloch I, Bendriem B, Lopez-Krahe J. Fast nonsupervised 3D registration of PET and MR images of the brain. *J Cereb Blood Flow Metab.* 1994;14:749–762.
23. Nikou C, Heitz F, Armspach JP, Namer IJ, Grucker D. Registration of MR/MR and MR/SPECT brain images by fast stochastic optimization of robust voxel similarity measures. *Neuroimage.* 1998;8:30–43.
24. Arnold S, Schlaug G, Niemann H, et al. Topography of interictal glucose hypometabolism in unilateral mesiotemporal epilepsy. *Neurology.* 1996;46:1422–1430.
25. Ho SS, Berkovic SF, McKay WJ, Kalnins RM, Bladin PF. Temporal lobe epilepsy subtypes: differential patterns of cerebral perfusion on ictal SPECT. *Epilepsia.* 1996;37:788–795.
26. Rubin E, Dhawan V, Moeller JR, et al. Cerebral metabolic topography in unilateral temporal epilepsy. *Neurology.* 1995;45:2212–2223.
27. Ryvlin P, Cinotti L, Froment JC, et al. Metabolic patterns associated with non-specific magnetic resonance imaging abnormalities in temporal lobe epilepsy. *Brain.* 1991;114:2363–2383.
28. Choi D, Na DG, Byun HS, et al. White-matter change in mesial temporal sclerosis: correlation of MRI with PET, pathology, and clinical features. *Epilepsia.* 1999;40:1634–1641.
29. Meiners LC, Witkamp TD, de Kort GA, et al. Relevance of temporal lobe white matter changes in hippocampal sclerosis: magnetic resonance imaging and histology. *Invest Radiol.* 1999;34:38–45.
30. Mitchell LA, Jackson GD, Kalnins RM, et al. Anterior temporal abnormality in temporal lobe epilepsy: a quantitative MRI and histopathologic study. *Neurology.* 1999;52:327–336.
31. Ryvlin P, Guenot M, Isnard J, et al. The role of the temporo-polar cortex in temporal lobe epilepsy [abstract]. *Stereotact Funct Neurosurg.* 1997;67:143.
32. Mesulam MM, Mufson EJ. Insula of the old world monkey. I. Architectonics in the insulo-orbito-temporal component of the paralimbic brain. *J Comp Neurol.* 1982;212:1–22.
33. Mesulam MM, Mufson EJ. Insula of the old world monkey. III. Efferent cortical output and comments on function. *J Comp Neurol.* 1982;212:38–52.
34. Rowe CC, Berkovic SF, Austin MC, McKay WJ, Bladin PF. Patterns of postictal cerebral blood flow in temporal lobe epilepsy: qualitative and quantitative analysis. *Neurology.* 1991;41:1096–1103.
35. Avery RA, Spencer SS, Spanaki MV, Corsi M, Seibyl JP, Zubal IG. Effect of injection time on postictal SPET perfusion changes in medically refractory epilepsy. *Eur J Nucl Med.* 1999;26:830–836.
36. Henry TR, Mazziotta JC, Engel J Jr. Interictal metabolic anatomy of mesial temporal lobe epilepsy. *Arch Neurol.* 1993;50:582–589.
37. Khan N, Leenders KL, Hajek M, Maguire P, Missimer J, Wieser HG. Thalamic glucose metabolism in temporal lobe epilepsy measured with ^{18}F-FDG positron emission tomography (PET). *Epilepsy Res.* 1997;28:233–243.
38. Sperling MR, Gur RC, Alavi A, et al. Subcortical metabolic alterations in partial epilepsy. *Epilepsia.* 1990;31:145–155.
39. Velasco M, Velasco F, Velasco AL, Lujan M, Vazquez del Mercado J. Epileptiform EEG activities of the centromedian thalamic nuclei in patients with intractable partial motor, complex partial, and generalized seizures. *Epilepsia.* 1989;30:295–306.
40. Henry TR, Votaw JR, Pennell PB, et al. Acute blood flow changes and efficacy of vagus nerve stimulation in partial epilepsy. *Neurology.* 1999;52:1166–1173.

SOCIETY OF NUCLEAR MEDICINE

Downloaded from jnm.snmjournals.org by on March 14, 2017. For personal use only.

JNM The Journal of NUCLEAR MEDICINE

Correlation Between PET and SISCOM in Temporal Lobe Epilepsy

Viviane Bouilleret, M. Paola Valenti, Edouard Hirsch, Franck Semah and Izzie J. Namer

J Nucl Med. 2002;43:991-998.

This article and updated information are available at:
http://jnm.snmjournals.org/content/43/8/991

Information about reproducing figures, tables, or other portions of this article can be found online at:
http://jnm.snmjournals.org/site/misc/permission.xhtml

Information about subscriptions to JNM can be found at:
http://jnm.snmjournals.org/site/subscriptions/online.xhtml

The Journal of Nuclear Medicine is published monthly.
SNMMI | Society of Nuclear Medicine and Molecular Imaging
1850 Samuel Morse Drive, Reston, VA 20190.
(Print ISSN: 0161-5505, Online ISSN: 2159-662X)

© Copyright 2002 SNMMI; all rights reserved.

SNMMI SOCIETY OF NUCLEAR MEDICINE AND MOLECULAR IMAGING